Organic coating on sulfate and soot particles during late summer in the Svalbard Archipelago

Hua Yu[1,2], Weijun Li[2*], Yangmei Zhang[3], Peter Tunved[4], Manuel Dall'Osto[5], Xiaojing Shen[3], Junying Sun[3], Xiaoye Zhang[3], Jianchao Zhang[6], Zongbo Shi[7,8*]

[1]College of Life and Environmental Sciences, Hangzhou Normal University, 310036, Hangzhou, China

[2]Department of Atmospheric Sciences, School of Earth Sciences, Zhejiang University, 310027, Hangzhou, China

[3]Key Laboratory of Atmospheric Chemistry, Chinese Academy of Meteorological Sciences, Beijing, China

[4]Department of Environmental Science and Analytical Chemistry, Stockholm University, 10691, Stockholm, Sweden

[5]Institute of Marine Sciences, ICM-CSIC, Passeig Marítim de la Barceloneta, 37-49, E-08003, Barcelona, Spain

[6]Key Laboratory of the Earth's Deep Interior, Institute of Geology and Geophysics, Chinese Academy of Sciences, 100029, China

[7]School of Geography, Earth and Environmental Sciences, the University of Birmingham, Birmingham, UK

[8]Institute of Surface Earth System Science, Tianjin University, Tianjin, China

[*]Corresponding Emails: liweijun@zju.edu.cn; z.shi@bham.ac.uk

Abstract

Interaction of anthropogenic particles with radiation and clouds plays an important role on Arctic climate change. Mixing state of aerosols is a key parameter to influence aerosol radiation and aerosol-cloud interaction. However, little is known on this parameter in the Arctic, preventing an accurate representation of this information in global models. Here we used transmission electron microscopy with energy-dispersive X-ray spectrometry, scanning electron microscopy, nanoscale secondary ion mass spectrometry, and atomic forces microscopy to determine the size and mixing state of individual sulfate and carbonaceous particles at 100 nm – 2 μm collected in the Svalbard Archipelago in summer. We found that 74% by number of non-sea salt sulfate particles were coated with organic matter (OM). 20% of sulfate particles also had soot inclusions which only appeared in the OM coating. The OM coating is estimated to contribute to 63% of the particle volume on average. To understand how OM coating influences optical properties of sulfate particles, a Mie core-shell model was applied to calculate optical properties of individual sulfate particles. Our result shows that absorption cross section of individual OM-coated particles significantly increased when assuming the OM coating as light-absorbing brown carbon. Microscopic observations here suggest that OM modulates the mixing structure of fine Arctic sulfate particles, which may determine their hygroscopicity and optical properties.

1. Introduction

Surface temperatures are rising faster in the Arctic than the rest of globe (IPCC, 2013). Although increased human-induced emissions of long-lived greenhouse gases are certainly one of the driving factors, air pollutants, such as aerosols and ozone, are also important contributors to climate change in the Arctic (Law and Stohl, 2007; Shindell, 2007). Spatial and temporal variations of aerosol composition, size distribution, and sources of Arctic aerosols have been studied extensively in numerous ground-based, ship, airborne observations, and various atmospheric models (Brock et al., 2011; Burkart et al., 2017; Chang et al., 2011; Dall'Osto et al., 2017; Fu et al., 2008; Hara et al., 2003; Hegg et al., 2010; Iziomon et al., 2006; Karl et al., 2013; Lathem et al., 2013; Leck and Bigg, 2008; Leck and Svensson, 2015; Moore et al., 2011; Raatikainen et al., 2015; Wöhrnschimmel et al., 2013; Winiger et al., 2017; Yang et al., 2018; Zangrando et al., 2013). These studies show that regional pollutants and local natural aerosol production affect sea ice albedo and the heat balance of the atmosphere, especially in the summer when mid-latitude transport is not as frequent relative to that during the winter/spring Arctic Haze season (Hansen and Nazarenko, 2004; Jacob et al., 2010; Shindell, 2007).

Aerosol particles in the Arctic atmosphere are mainly composed of sea salt, sulfate, particulate organic matter (OM) with a small amount of ammonium, nitrate, black carbon (BC) (Hara et al., 2003; Quinn et al., 2007) and mineral dust particles (Dagsson-Waldhauserova et al., 2013). Sea salts, derived from the Arctic Ocean, are the dominant coarse particles (>1 μm) in the Arctic atmosphere (Behrenfeldt et al., 2008; Chi et al., 2015). Compared to other types of aerosols, sea salt is the largest contributor to radiative forcing in remote Ocean air (Wang et al., 2019). Natural sea salt particles can provide large surfaces for heterogeneous reaction with acidic gases in the Arctic air (Chi et al., 2015; Geng et al., 2010; Hara et al., 2003). Moreover, sea salt particles are an important source of cloud condensation nucleation (CCN) in the Arctic air (Abbatt et al., 2019); Coarse dust particles in the Svalbard region have been observed to be occasionally influenced from local (Svalbard) and/or distant (e.g., Iceland, Greenland and Siberia) sources in high latitudes (Behrenfeldt et al., 2008).

Tobo et al. (2019) showed that glacial outwash sediments in Svalbard (a proxy for glacially sourced dusts) due to the recent rapid and widespread retreat of glaciers have a remarkably high ice nucleating ability under conditions relevant for mixed-phase cloud formation.

BC, commonly called ‘‘soot’’, is derived from the combustion sources such as diesel engines, residential solid fuel, and open burning (Bond et al., 2013). Studies show BC in the Arctic absorbs solar radiation in the atmosphere and when deposited on snow (Iziomon et al., 2006; Koch and Hansen, 2005; Sand et al., 2013; Shindell, 2007). Maahn et al. (2017) found that BC concentration is enhanced below the clouds in the Arctic. This influences the mean effective radii of cloud droplets which lead to the suppressed drizzle production and precipitation. Possible sources of BC particles in the Arctic include natural gas flaring (Qi et al., 2017), ship emissions (Browse et al., 2013; Weinbruch et al., 2012) and long range transport from emissions of biomass burning and fossil fuels in the northern hemisphere (Winiger et al., 2016; Xu et al., 2017). Winiger et al.(2017) showed that most of the Arctic BC is from domestic activities (35%) and transportation (38%), with only minor contributions from gas flaring (6%), power plants (9%), and open fires (12%).

OM is a significant component in Arctic aerosol (Quinn et al., 2007). More than 100 organic species have been detected in the Arctic aerosols and polyacids are the most abundant compound class, followed by phthalates, aromatic acids, fatty acids, fatty alcohols, sugars/sugar alcohols, and n-alkanes (Fu et al., 2008). Recently, certain organic aerosols, referred to as brown carbon (BrC), have been recognized as an important light-absorbing carbonaceous aerosol in the troposphere (Alexander et al., 2008; Andreae and Gelencser, 2006; Feng et al., 2013; Lack et al., 2012). BrC can be directly emitted from combustion sources or form in the atmosphere via photo-chemical aging (Jiang et al., 2019; Saleh et al., 2013; Updyke et al., 2012). Moreover, aging of secondary organic aerosols can significantly contribute to BrC during atmospheric transport (Laskin et al., 2015). Feng et al.(2013) estimated that on average, BrC accounts for 66% of total OM mass globally and its light absorption is about 26% of BC.

Sulfate is a dominant aerosol component in the Arctic air (Quinn et al., 2007). The Community Earth System Model simulations show that sources from East Asia have the largest contribution to the Arctic sulfate column burden, with an annual mean contribution of 27%, followed by 11–13% each from South Asia, the rest of the world (including the Arctic), and Russia/Belarus/Ukraine sources and 13% from natural sources (Yang et al., 2018). Large amounts of secondary species including sulfate and OM not only change radiative forcing and number of CCN in Arctic atmosphere (Abbatt et al., 2019; Yang et al., 2018) but also influence optical, hygroscopic, and CCN activity of these internally mixed BC and mineral dust particles (Lathem et al., 2013; Raatikainen et al., 2015; Zanatta et al., 2018).

BC and BrC are often internally mixed with other non-absorbing aerosols, such as sulfate (Lack et al., 2012; Laskin et al., 2015). Internal mixing means that a single particle simultaneously contains two or more types of aerosol components (Li et al., 2016). This internal mixing can enhance BC absorption by a factor of two (Bond et al., 2013) and change the activity of CCN in the Arctic atmosphere (Leck and Svensson, 2015; Martin et al., 2011). A few previous studies also looked at the mixing states of coarse aerosol particles in Arctic troposphere (Behrenfeldt et al., 2008; Chi et al., 2015; Geng et al., 2010; Hara et al., 2003; Leck and Svensson, 2015; Moroni et al., 2017; Raatikainen et al., 2015; Sierau et al., 2014), but those of fine non-sea salt particles, including the most important short-lived climate forcers – BC and BrC (Feng et al., 2013; Fu et al., 2008; Kirpes et al., 2018; Laskin et al., 2015; Leck and Svensson, 2015), are poorly characterized. A poor understanding on mixing state of BC and BrC in individual particles prevents an accumulate simulation of the direct aerosol forcing and aerosol-cloud interaction in the Arctic (Browse et al., 2013; Samset et al., 2014; Zanatta et al., 2018).

In this study, individual aerosol particles were collected in Svalbard during 7-23 August, 2012. We combined the data from various microscopic instruments to determine the size, composition, and mixing properties of individual particles, with a particular focus on sulfate and carbonaceous particles. Mie theory was used to test how OM coating influences optical properties of sulfate particles in the Arctic when

OM was assumed as BrC. The results are discussed in the context of aerosol radiation and aerosol-cloud interaction.

2. Experimental section

2.1 Field campaign

The Svalbard archipelago includes all landmasses between 74 and 81 degrees North and 10 and 35 degrees East (Figure 1). The islands cover 63000 km^2. Ny-Ålesund town is situated on the west coast of the largest island, Spitsbergen and 1200 km from the North Pole. It is a central platform for Arctic research.

The observation site is based at the Chinese Arctic Yellow River Station (78°55′N, 11°56′E) (Chi et al., 2015; Geng et al., 2010). The site is about 2 km far away from the Zeppelin observatory station (78.9N 11.88E) run by the Ny-Ålesund Science Managers Committee. On the west coast of the island of Spitsbergen, Ny-Ålesund is a Norwegian research and monitoring infrastructure, hosting national and international research projects and programmes. The Norwegian Polar Institute (NPI) runs the Sverdrup Research Station at the coast and Zeppelin Observatory at the Mountain 475 m asl, and Sweden, Germany, France, Italy, Japan, China, England, The Netherlands, South Korea, and India are the other countries to have established long-term programmes in Ny-Ålesund (https://www.esrl.noaa.gov/psd/iasoa/stations/nyalesund). Two to three samples were regularly collected at 9:00, 16:00, 21:00 (local time) of each day, with a total of 46 samples during 7-23 August, 2012.

A sampler containing a single-stage impactor with a 0.5-mm-diameter jet nozzle (Genstar Electronic Technology, China) was used to collect individual particles by the air flow rate at 1.5 l min^{-1}. Aerosol particles were collected onto copper TEM grids coated with carbon film. This sampler has a collection efficiency of 31% at 100 nm aerodynamic diameter and 50% at 200 nm assuming the density of the particles is 2 g cm^{-3}. Sampling times varied from twenty minutes to two hours depending on the loading of particles. After collection, each sample was placed in a sealed dry plastic tube and stored in a desiccator at 20 ± 3% RH for analysis. Ambient laboratory conditions (17−23% RH and 19−21 °C) is effective at preserving individual

hygroscopic aerosol particles and reducing changes that would alter samples and subsequent data interpretation (Laskina et al., 2015). During the sampling period, meteorological data at the sampling site including pressure (P), relative humidity (RH), temperature (T), wind speed (WS), and wind direction (WD) were recorded every 5 min using a pocket weather meter (Kestrel 4500, Nielsen-Kellermann Inc., USA). Sample information including local sampling date and time and various meteorological conditions are listed in Table 1.

2.2 TEM measurement

Individual particle samples were examined by a JEOL JEM-2100 transmission electron microscopy operated at 200 kV with an energy-dispersive X-ray spectrometry (TEM/EDS). TEM can observe the mixing structure of different aerosol components within an individual particle on the substrate because electron beam transmit through the specimen to form an image. EDS spectra are acquired for a maximum time of 30 s to minimize potential beam damage and collect particle X-ray spectra with sufficient intensity. TEM grids are made of copper (Cu) and covered by a carbon-reinforced substrate, so Cu is excluded from the quantitative analyses of the particles. Because of the substrate contribution, C content in TEM grid coated by carbon film might be overestimated in EDS spectra of individual particles.

The distribution of aerosol particles on TEM grids was not uniform, with coarser particles occurring near the center and finer particles on the periphery. Therefore, to ensure that the analysed particles are representative, five areas were chosen from the center to periphery of the sampling spot on each grid. Through a labor-intensive operation, 2002 aerosol particles with diameter < 10 μm in 21 samples were analysed by TEM/EDS (Table 1). To check elemental composition of individual particles, EDS was manually used to obtain elemental spectra of individual particles. In the clean Arctic air, there are simple particle types including sea salt, sulfate, soot, OM, and mineral. Because soot particles have chain-like aggregation, it is not necessary to check their elemental composition. Sea salt particles display spherical or square shapes and are stable under the electron beam in TEM (Chi et al., 2015). Sulfate

particles are spherical but flats on the substrate and produce unstable bubble under the electron beam (Buseck and Posfai, 1999). TEM observations can also identify sulfate particles or sulfate with OM coating. TEM/EDS analysis is very time-consuming. Thus, we did not check the composition of every single particle analysed. Instead, we randomly checked the elemental composition of 20-30 particles in each sample (Table 1). EDS spectra of 575 particles were manually selected and saved in the computer for elemental composition analysis. Particles examined by TEM were dry at the time of observation in the vacuum of the electron microscope. In our study, the effects of water and other semi-volatile organics were not considered as they evaporated in the vacuum.

Elemental mapping and line profile of selected individual aerosol particles were also obtained from the EDS scanning operation mode of TEM (STEM). The STEM information clearly display elemental distribution in the targeted individual particles which cannot be provided by the above EDS analysis. Based on preliminary individual analysis, we further chose the typical samples containing abundant sulfate with OM coating for the STEM analysis. High-resolution elemental distribution in individual particles provides detailed mixing structure of sulfate and OM in individual particles.

The iTEM software (Olympus soft imaging solutions GmbH, Germany) is an image analysis platform for electron microscopy. In this study, it was used to manually or automatically obtain area, perimeter, and equivalent circle diameter (ECD) of individual particles. In these analysed samples, we found there were abundant sulfate particles (~30% by number) in the 11 samples collected during 9-15 August, 2012. In other samples, there are more sea salt particles with few particles. Based on the TEM observations, we selected the samples containing more sulfate particles for further microscopic analyses (see below).

2.3 NanoSIMS measurement

Because the sulfate particles in different samples collected in the Arctic had similar elemental composition and mixing state from the TEM observations, we

selected three samples (Table 1) for nanoscale secondary ion mass spectrometry (NanoSIMS) analysis (CAMECA Instruments, Geneviers, France). A micro-cesium source was used to generate Cs^+ primary ions, with an impact energy of 16 kV for sample interrogation. The primary beam was stepped across the sample to produce element specific, quantitative digital images. The Cs^+ primary ion beam was used to obtain $^{16}O^-$, $^{12}C^{14}N^-$, $^{14}N^{16}O^-$, $^{32}S^-$, $^{35}Cl^-$, and $^{16}O^{23}Na^-$ ions in this study. The NanoSIMS analysis can obtain ion mapping of particles with nanometer spatial resolution over a broad range of particle sizes (Figure S1). Because the substrate of TEM grid is carbon, CN^- is adopted to represent OM in individual particles (Chi et al., 2015; Ghosal et al., 2014). S^- is used to infer the presence of sulfates in individual particles (Li et al., 2017). A total of 32 sulfate containing particles were analysed by the NanoSIMS.

2.4 SEM measurement

We used a Zeiss ultra 55 scanning electron microscopy (SEM) with EDS to examine the vertical distribution of OM and sulfate in individual particles. TEM grids were mounted onto an aluminum SEM stub and directly observed in secondary electron image mode. SEM analysis was operated at 10 kv of extra high tension (EHT) and 9.7 mm of work distance (WD). Processes such as sample moving, analysis region selection and imaging were controlled by computer. The specimen stage in SEM was tilted at the range of 0-75^o, and then we vertically observed thickness of OM coating and sulfate core on the substrate. Two typical samples that contain abundant sulfate particles were chosen for this analysis (Table 1).

2.5 AFM measurement

AFM with a digital nanoscope IIIa instrument operating in the tapping mode was used to observe surface morphology of individual aerosol particles and measure particle thickness. The tapping AFM has a cantilever and conical tip of 10 nm radius. By using AFM, a general image of the particles is taken at 10 μm full scan size, which generally includes 1-2 particles depending on the exact location. In this study, we are only interested in the sulfate-containing particles. AFM provides surface information

and morphology of 17 particles but no composition. Samples were firstly quickly examined by the TEM under low magnification mode to find sulfate-containing particles. Because TEM grids have coordinates letters, we can find the same particles in the AFM. This analysis provides 3-D image of the sulfate-containing particles and their volume. After we obtained AFM images of sulfate particles, the NanoScope analysis software can automatically obtain bearing area (A) and bearing volume (V). This can then be converted into equivalent circle diameter (d, ECD) and equivalent spherical diameter (D, ESD)

$$A = \frac{4}{3}\pi r^2 = \frac{\pi d^2}{3} \rightarrow d = \sqrt{\frac{3A}{\pi}} \quad (1)$$

$$V = \frac{4}{3}\pi r^3 = \frac{4}{3} \times \frac{\pi D^3}{8} \rightarrow D = \sqrt[3]{\frac{6V}{\pi}} \quad (2)$$

ESD and ECD of sulfate-containing particles are well corrected. Using the linear correlation equation (ESD=0.38ECD), we can then correct the ESD of individual particles from TEM analysis to obtain the ECD (Chi et al., 2015).

2.6 Calculation of BrC optical properties

The refractive index used for the non-light-absorbing sulfate component was set to m=1.55 at 550 nm (Seinfeld and Pandis, 2006). The refractive index of OM (as BrC) is not known so we considered three scenarios: strongly absorbing (1.65-0.03i at 550 nm), moderately absorbing (1.65-0.003i at 550 nm), and non-absorbing OM (1.65 at 550 nm) (Feng et al., 2013). Here, we choose 550 nm as a case study to test how OM coating influence sulfate particles in Arctic air.

BHCOAT Mie code by Bohren and Huffman (1983) was used to calculate the optical properties, including scattering cross section (SCS), absorption cross section (ACS), and single scattering albedo (SSA), assuming a core-shell structure. We firstly calculated these parameters assuming a sulfate core and OM shell structure only (ignoring some of the particles that contain soot core). Because the Mie code only can calculate the core-shell structure or homogeneous model, we assume sulfate as a core and OM as a shell in individual particle to build the core-shell model. Based on the

core-shell standard mode (Li et al., 2016), we can calculate optical properties of individual internally mixed particles.

2.7 Back trajectories of air masses and Lagrangian particle dispersion model

Three-day (72 h) back trajectories of air masses were generated using a Hybrid Single Particle Lagrangian Integrated Trajectory (HYSPLIT) model at the Chinese Arctic Yellow River Station during August 2012. Here we selected an altitude of 500 m as the end point in each back trajectory (Figure 1). Back trajectories for 50 m and 1000 m above sea level are similar.

A lagrangian particle dispersion model FLEXPART-WRF 3.1 (Brioude et al., 2013) was also used to examine the origin of particles. The FLEXPART-WRF model is using meteorological parameters from WRF dynamical simulation. The domain resolution is 50×50 km with 64 vertical levels. The FLEXPART-WRF simulations were launched in a backward mode over 10 days, with the Chinese Arctic Yellow River Station as an origin. For each simulation (one per sample), 20000 pseudo-particles were released in a small volume around the station position. Each single particle position evolution backward in time was determined by Lagrangian dispersion calculation.

Based on the TEM experiments and back trajectory of air masses (Figure 1), we found that there were more S-rich with OM coating particles in the samples collected on August 11, 12, 14, and 15, 2012. Therefore, we further did the FLEXPART-WRF simulation of these four days (Figure 2). The emission intensity in the Arctic area has been also shown in Figure S2.

3. Results

3.1 Composition and source of aerosol particles

TEM/EDS analysis shows that O, Na, S, and Cl are dominant elements in individual particles (Figure S3). On basis of the composition and morphology of individual particles, we classified the particles into four major groups: Na-rich (i.e. NaCl, Na_2SO_4, and $NaNO_3$), S-rich (i.e. ammonium sulfate and sulfuric acid), carbonaceous (soot and OM), and mineral dust particles. The classification criteria of different particle types and their sources have been described in a separate study (Li et

al., 2016). S-rich particles representing secondary inorganic particles (e.g., SO_4^{2-}, NO_3^-, and NH_4^+) are converted from gaseous SO_2, NO_x, and NH_3. OM can be divided into primary organic matter (POM) and secondary organic matter (SOM). SOM is produced from the chemical oxidation of volatile organic compounds (VOCs) and often exhibits OM coating on S-rich particles (Li et al., 2016; Moffet et al., 2013; Riemer et al., 2019). Na-rich particles in the marine air are from sea spray and have typical near cubic shape. Mineral dust particles from natural ground soil contain Si, Al, or Ca and have irregular shape. Soot particles, which contain C with minor O, appear as a chain-like aggregate of carbon-bearing spheres. Chi et al. (2015) studied the aging mechanism of sea salt particles. Here, we focused on non-sea salt (NSS) particles including S-rich, soot, and OM particles NSS-particles and sulfate-containing particles account for 39±5% and 29±7% by number of all the 2002 particles analysed (Figure 3).

3.2 OM coating on sulfate particles

TEM observations revealed a common core-shell mixing structure in fine sulfate-containing particles (Figure 4a). Elemental mapping of such internally mixed sulfate particles shows C signals in the coating (C map, Figure 4b) and S and O signals in the center (S and O map, Figure 4c, d). The elemental line profile of a sulfate particle also shows sulfate core and C coating (Figure S4). Furthermore, ion maps of individual particles from the NanoSIMS further show $^{12}C^{14}N^-$ signals in the coating (red color in Figure 4e, f) and $^{32}S^-$ signals in the core (green color in Figure 4e, g). These results provide strong evidence that the coating is OM and the core is sulfate.

A majority of the 781 analysed NSS-particles (74% by particle number) have a sulfate core and OM coating (Figures 4 and 5). ~20% of them also contain small soot inclusions but they only appeared in organic coating, rather than as the core (Figure 5b). The mixing structure is different from our previous findings in polluted air where soot is normally mixed with sulfate instead of OM coating (Li et al., 2016). Moreover, we observed some chain-like soot aggregates (1.3% in all analysed particles) (Figure

S5) but they only occurred in three samples during the whole sampling period (Table 1). Considering the remoteness of the sampling site, such fresh soot particles are likely to be of local origin, for example, shipping and flaring (Gilgen et al., 2018; Peters et al., 2011).

TEM observations showed that some sulfate-containing particles had unique morphology that a sulfate particle was surrounded by some smaller particles (Figure 5a). They are often called "satellite" particles as they were distributed from the central particles when impacted on the substrate during sample collection. Satellite particles were observed around 16% of the analysed sulfate-containing particles (Figure 5a) in the samples (Table 1) collected during 9-15 August. NanoSIMS analysis further showed that the satellite particles (Table 1) have strong $^{32}S^-$ (Figure 6a, c) and $^{16}O^-$ signals (Figure 6d) as well as weak $^{12}C^{14}N^-$ signals (Figure 6a, b). Previous studies showed that the similar satellite particles are normally considered as acidic sulfate (Buseck and Posfai, 1999; Iwasaka et al., 1983). Our results show that these acidic satellites not only contain sulfuric acid but also some OM or organic acids. Indeed, Fu et al. (2008) found that polyacids are the most abundant organic compounds, followed by phthalates, aromatic acids, and fatty acids in Arctic aerosol particles. Based on the back trajectories of air masses and FLEXPART modelling, most air masses originate in the North America and Greenland during the sampling periods (Figures 1 and 2). Figure 1 shows that these air masses brought abundant sulfate-containing particles into the sampling area in summertime.

AFM was used to obtain 3D image of individual secondary particles impacting on the substrate. Figure 7a shows that the secondary particles normally have smooth surface which is different from uneven surface of the Arctic fresh and aged NaCl particles (Chi et al., 2015). Furthermore, we observed particle thickness through tilting the specimen stage up to 75^o in SEM. Figure 7a-b both shows that the secondary particles look like thin pancake sticking on the substrate. Furthermore, the sections of two secondary particles in the AFM images shows that the highest heights of particles are only 15% (green line) and 26% (red line) of the corresponding horizontal diameter (Figure 7a). These results show that the shape of individual

particles was modified when they impacted on the substrate following the airflow. Therefore, the measured ECDs of individual particles in TEM images are much larger than the real particle diameter. To calibrate the particle diameter, we obtained volume of dry particles on the substrate and then calculated their ESD in the AFM images (Figure 7c). ESD distribution of the secondary Arctic particles displayed a peak at 340 nm, ranging from 100 nm to 2000 nm (Figure 7d). The core particles, as sulfate or soot, had a peak at 240 nm and 120 nm, respectively (Figure 7d). It is estimated that OM on average accounted for 63±23% of the dry sulfate-containing particle volume. Our result shows that the OM volume increases following the particle size increase (Figure S6).

4. Discussion

4.1 Mixing mechanism of organic, soot, and sulfate

Lagrangian particle dispersion modeling using the FLEXPART-WRF 3.1 showed that air masses arriving at the sampling site during our field measurement periods were likely originated from the Greenland and North America (Figure 2). Previous studies reported that air masses from North America or Greenland during the summer contain higher concentration of black carbon, OM, and sulfate (Burkart et al., 2017; Chang et al., 2011; Fu et al., 2008; Moore et al., 2011; Park et al., 2013). Indeed, there is strong emission intensity of OC and SO_2 around the Arctic area from emission simulation as shown in Figure S2. However, Weinbruch et al. (2012) observed soot particles when cruise ships were present in the area around Ny-Ålesund town. It is possible that minor soot particles are from the ship emissions and most of them are transported from outside Arctic area in the free troposphere (Figure S2).

The sulfate core-OM shell structure observed in the Arctic summer atmosphere is similar to those in the background or rural air in other places (Li et al., 2016; Moffet et al., 2013). Based on the images from electron microscopies, we can infer that OM coating thickness in the Arctic air was comparable with them in rural places but higher than them in urban places. During the transports, organic coatings on sulfate were considered as the SOM and their masses increase following particle aging and

403 growth (Li et al., 2016; Moffet et al., 2013; Sierau et al., 2014). Figures 1 and 2 show
404 that most of particles in the air masses are transported from North American. The
405 sulfate/OM particles with soot inclusions are probably formed in a similar way as
406 those found elsewhere (Li et al., 2016) – e.g., soot particles may have acted as nuclei
407 for secondary sulfate or organic uptake during their transports (Riemer et al., 2009).
408 Similarly, besides the OM coating in the Arctic particles, Leck and Svensson (2015)
409 found biogenic aerosols like gel-aggregate containing bacterium in ultrafine particles.
410 However, we did not find any gel-like particles in the samples because our sampler
411 had very low efficiency for ultrafine particles.

412 TEM images show that most of the internally mixed sulfate-containing particles
413 display sulfate core and OM coating on the substrate (Figures 4a and 5b, c).
414 Knowledge on the phase separation in individual particles is important to understand
415 particle hygroscopic properties, heterogeneous reactions of reactive gases on particle
416 surface, and organic aging (You et al., 2012). It is possible that the thick OM coatings
417 were consistently built up during the long-range transport of sulfate-containing
418 particles and part of the SOM in the coating likely formed in Arctic area. Indeed, there
419 are various sources of organic precursors during the Arctic area, such as biogenic
420 VOCs from ice melting and open water (Dall Ὅsto et al., 2017) and anthropogenic
421 VOCs from shipping emissions in summertime (Gilgen et al., 2018). The dependence
422 of OM volume on particle size (Figure S6) suggests that the suspended sulfate
423 particles are initially important surface for SOM formation. Moreover, the presence of
424 OM coating in 74% sulfate particles indicates that SOM as the surfaces of fine
425 particles may govern the possible heterogeneous reactions between reactive gases and
426 sulfate-containing particles in the Arctic air.

427 It should be noted that most of SOM not only occurred on the surfaces of
428 sulfate-containing particles but also its mass (mean mass at 63±23%) dominated in
429 individual particles (Figure 7d). The OM dominating in individual particles can
430 influence the IN and CCN activities of secondary sulfate-containing particles (Lathem
431 et al., 2013; Martin et al., 2011). For example, some studies found that an increase in
432 organic mass fraction in particles of a certain size would lead to a suppression of the

Arctic CCN activity (Leck and Svensson, 2015; Martin et al., 2011). Moreover, OM as particle surfaces can significantly influence hygroscopicity and IN activity of sulfate-containing particles (Wang et al., 2012).

4.2 Potential impact of OM on optical properties of sulfate-containing particles

The internal mixing of soot, sulfate, and OM can change optical properties of individual particles in the atmosphere. Recent studies showed that BrC has been detected in the OM in the polluted and clean air and even in upper troposphere (Laskin et al., 2015; Wang et al., 2018). Feng et al. (2013) further calculated the contribution up to 19% of the optical absorption of the strongly absorbing BrC in global simulations which is after the absorption BC aerosols. Various colored OM (e.g. nitrated/polycyclic aromatics and phenols), referred as BrC, were detected in the Arctic atmosphere in different seasons (Fu et al., 2008; Wöhrnschimmel et al., 2013; Zangrando et al., 2013) and in surface ice or snowpack (Browse et al., 2013; Doherty et al., 2013; Hegg et al., 2010). We also noticed that the $^{12}C^{14}N^-$ signal occurred in all analysed OM coating in sulfate-containing particles (Figure 4e-f). $^{12}C^{14}N^-$ from NanoSIMS is indicative of the presence of nitrogen-containing organic in the detected materials (Herrmann et al., 2007). Figure 4 showed that the nitrogen-containing OM was more or less homogeneously distributed in the OM coating in individual particles. This suggests that some of the OM in the coating has the potential to act as BrC (Jiang et al., 2019; Laskin et al., 2015).

To understand how OM coating influence optical properties of sulfate-containing particles, we make an assumption that OM coating is strongly absorbing (case 1), moderately absorbing (case 2) or non-absorbing BrC (case 3) with a refractive index of 1.65-0.03i, 1.65-0.003i, and 1.65 at 550 nm according to Feng et al. (2013). Based on the size measurements shown in Figure 7d, we can calculate volume of sulfate and OM within each particle. We input volume of each component and the corresponding refractive index into the Mie code and then calculated optical properties of individual sulfate-containing particles in the samples. Based on optical data statistic of 575 particles, Figure 8a show that if the OM coating is strongly absorbing BrC (referred to

case Abs1), the average absorption cross section (ACS) of individual particles is estimated to be 2.67×10^{-14} m^2. This value is 8.30 times higher than the aerosol ACS (3.22×10^{-15} m^2) when assuming that the BrC is moderately absorbing (referred to case Abs2, Figure 8a). However, the scattering cross section (SCS) of individual particles only shows a small change (Figure 8b). Figure 8c also shows that the single scattering albedos (SSAs) of individual particles are 0.92, 0.99, and 1 when assuming the OM as strongly, moderately and non-absorbing BrC (cases SSA1 to SSA3). These results suggest that whether we consider organic coating as BrC may have a significant influence on the absorption properties of individual sulfate-containing particles.

In this study, we explored the relationship between ACS of individual particles and particle diameters. Interestingly, Figure 8d shows that ACS of individual fine OM-coating sulfate particles increased with particle size. This suggests that the ACS of individual particles may increase as they grow and age in the atmosphere.

Current climate models estimated the radiative force of Arctic BC (Sand et al., 2013; Shindell, 2007; Winiger et al., 2017; Zanatta et al., 2018), but none specifically considered optical properties of Arctic BrC. Our study revealed the OM coating on individual sulfate particles, which should be considered in aerosol radiation effect and cloud-aerosol interaction simulations in the models.

5 Summary

A range of individual particle observation techniques, such as TEM/EDS, STEM, SEM, NanoSIMS, and AFM, were applied to study S-rich, soot, and OM particles in the Arctic atmosphere in the summer 2012. Sulfate-containing particles account for approximately 29±7% by number of all analysed particles. TEM and NanoSIMS showed that individual sulfate-containing particles have OM coating with sulfate as core. The SOM on the surfaces of fine particles may affect heterogeneous reactions between reactive gases and sulfate particles in the Arctic air. Furthermore, 20% of the sulfate-containing particles also contain small soot inclusions but they only appeared in organic coating.

Size distribution of the secondary Arctic particles displayed a peak at 340 nm,

ranging from 100 nm to 2000 nm. The core particles, as sulfate or soot, had a peak at 240 nm and 120 nm, respectively. OM coating on average contribute 63±23% by volume to the dry NSS-particles. We also found that whether the OM coating may have a significant influence on the absorption properties of individual particles in the Arctic air, depending on the optical properties of the OM.

Author Contributions: WL and ZS designed the study. YZ and XS collected aerosol particles. WL, HY, and JZ contributed laboratory experiments and data analysis. HY and WL performed optical calculation and wrote part of first draft. PT and MD provided the online measurement data of new particle formation and growth. JS and XZ coordinated the field campaign. All authors commented and edited the paper.

Competing interests: The authors declare no competing financial interests

Acknowledgments We thank Boris Quennehen to provide data from the FLEXPART-WRF. This work was funded by National Natural Science Foundation of China (41622504, 41575116, 31700475) and the Hundred Talents Program in Zhejiang University, Z.S. acknowledges funding from NERC (NE/S00579X/1).

References

Abbatt, J.P.D., Leaitch, W.R., Aliabadi, A.A., Bertram, A.K., Blanchet, J.P., Boivin-Rioux, A., Bozem, H., Burkart, J., Chang, R.Y.W., Charette, J., Chaubey, J.P., Christensen, R.J., Cirisan, A., Collins, D.B., Croft, B., Dionne, J., Evans, G.J., Fletcher, C.G., Galí, M., Ghahremaninezhad, R., Girard, E., Gong, W., Gosselin, M., Gourdal, M., Hanna, S.J., Hayashida, H., Herber, A.B., Hesaraki, S., Hoor, P., Huang, L., Hussherr, R., Irish, V.E., Keita, S.A., Kodros, J.K., Köllner, F., Kolonjari, F., Kunkel, D., Ladino, L.A., Law, K., Levasseur, M., Libois, Q., Liggio, J., Lizotte, M., Macdonald, K.M., Mahmood, R., Martin, R.V., Mason, R.H., Miller, L.A., Moravek, A., Mortenson, E., Mungall, E.L., Murphy, J.G., Namazi, M., Norman, A.L., O'Neill, N.T., Pierce, J.R., Russell, L.M., Schneider, J., Schulz, H., Sharma, S., Si, M., Staebler, R.M., Steiner, N.S., Thomas, J.L., von Salzen, K., Wentzell, J.J.B., Willis, M.D., Wentworth, G.R., Xu, J.W., Yakobi-Hancock, J.D.: Overview paper: New insights into aerosol and climate in the Arctic, Atmos. Chem. Phys., 19 (4), 2527-2560, 2019.

Alexander, D.T.L., Crozier, P.A., Anderson, J.R.: Brown Carbon Spheres in East Asian Outflow and Their Optical Properties, Science, 321 (5890), 833-836, 2008.

Andreae, M.O., Gelencser, A.: Black carbon or brown carbon? The nature of light-absorbing carbonaceous aerosols, Atmos. Chem. Phys., 6 (10), 3131-3148, 2006.

Behrenfeldt, U., Krejci, R., Ström, J., Stohl, A.: Chemical properties of Arctic aerosol particles collected at the Zeppelin station during the aerosol transition period in May and June of 2004, Tellus B, 60 (3), 405-415, 2008.

Bohren, C.F., Huffman, D.R., 1983. Absorption and scattering of light by small particles. John Wiley & Sons, Inc. , New York, USA.

Bond, T.C., Doherty, S.J., Fahey, D.W., Forster, P.M., Berntsen, T., DeAngelo, B.J., Flanner, M.G., Ghan, S., Kärcher, B., Koch, D., Kinne, S., Kondo, Y., Quinn, P.K., Sarofim, M.C., Schultz, M.G., Schulz, M., Venkataraman, C., Zhang, H., Zhang, S., Bellouin, N., Guttikunda, S.K., Hopke, P.K., Jacobson, M.Z., Kaiser, J.W., Klimont, Z., Lohmann, U., Schwarz, J.P., Shindell, D., Storelvmo, T., Warren, S.G., Zender, C.S.: Bounding the role of black carbon in the climate system: A scientific assessment, J. Geophys. Res., 118 (11), 5380-5552, 2013.

Brioude, J., Arnold, D., Stohl, A., Cassiani, M., Morton, D., Seibert, P., Angevine, W., Evan, S., Dingwell, A., Fast, J.D., Easter, R.C., Pisso, I., Burkhart, J., Wotawa, G.: The Lagrangian particle dispersion model FLEXPART-WRF version 3.1, Geosci. Model Dev., 6 (6), 1889-1904, 2013.

Brock, C.A., Cozic, J., Bahreini, R., Froyd, K.D., Middlebrook, A.M., McComiskey, A., Brioude, J., Cooper, O.R., Stohl, A., Aikin, K.C., de Gouw, J.A., Fahey, D.W., Ferrare, R.A., Gao, R.S., Gore, W., Holloway, J.S., Hübler, G., Jefferson, A., Lack, D.A., Lance, S., Moore, R.H., Murphy, D.M., Nenes, A., Novelli, P.C., Nowak, J.B., Ogren, J.A., Peischl, J., Pierce, R.B., Pilewskie, P., Quinn, P.K., Ryerson, T.B., Schmidt, K.S., Schwarz, J.P., Sodemann, H., Spackman, J.R., Stark, H., Thomson, D.S., Thornberry, T., Veres, P., Watts, L.A., Warneke, C., Wollny, A.G.: Characteristics, sources, and transport of aerosols measured in spring 2008 during the aerosol, radiation, and cloud processes affecting Arctic Climate (ARCPAC) Project, Atmos. Chem. Phys., 11 (6), 2423-2453, 2011.

Browse, J., Carslaw, K.S., Schmidt, A., Corbett, J.J.: Impact of future Arctic shipping on high-latitude black carbon deposition, Geophys. Res. Lett.,, 40 (16), 4459-4463, 2013.

Burkart, J., Willis, M.D., Bozem, H., Thomas, J.L., Law, K., Hoor, P., Aliabadi, A.A., Köllner, F., Schneider, J., Herber, A., Abbatt, J.P.D., Leaitch, W.R.: Summertime observations of elevated levels of ultrafine particles in the high Arctic marine boundary layer, Atmos. Chem. Phys., 17 (8),

5515-5535, 2017.

Buseck, P.R., Posfai, M.: Airborne minerals and related aerosol particles: Effects on climate and the environment, P. Natl. Acad. Sci. USA, 96 (7), 3372-3379, 1999.

Chang, R.Y.W., Leck, C., Graus, M., Müller, M., Paatero, J., Burkhart, J.F., Stohl, A., Orr, L.H., Hayden, K., Li, S.M., Hansel, A., Tjernström, M., Leaitch, W.R., Abbatt, J.P.D.: Aerosol composition and sources in the central Arctic Ocean during ASCOS, Atmos. Chem. Phys., 11 (20), 10619-10636, 2011.

Chi, J.W., Li, W.J., Zhang, D.Z., Zhang, J.C., Lin, Y.T., Shen, X.J., Sun, J.Y., Chen, J.M., Zhang, X.Y., Zhang, Y.M., Wang, W.X.: Sea salt aerosols as a reactive surface for inorganic and organic acidic gases in the Arctic troposphere, Atmos. Chem. Phys., 15 (19), 11341-11353, 2015.

Dagsson-Waldhauserova, P., Arnalds, O., Olafsson, H.: Long-term frequency and characteristics of dust storm events in Northeast Iceland (1949–2011), Atmos. Environ., 77 (0), 117-127, 2013.

Dall'Osto, M., Beddows, D.C.S., Tunved, P., Krejci, R., Ström, J., Hansson, H.C., Yoon, Y.J., Park, K.-T., Becagli, S., Udisti, R., Onasch, T., O'Dowd, C.D., Simó, R., Harrison, R.M.: Arctic sea ice melt leads to atmospheric new particle formation, Sci. Rep., 7 (1), 3318, 2017.

Doherty, S.J., Grenfell, T.C., Forsström, S., Hegg, D.L., Brandt, R.E., Warren, S.G.: Observed vertical redistribution of black carbon and other insoluble light-absorbing particles in melting snow, J. Geophys. Res., 118 (11), 5553-5569, 2013.

Feng, Y., Ramanathan, V., Kotamarthi, V.R.: Brown carbon: a significant atmospheric absorber of solar radiation?, Atmos. Chem. Phys., 13 (17), 8607-8621, 2013.

Fu, P., Kawamura, K., Barrie, L.A.: Photochemical and Other Sources of Organic Compounds in the Canadian High Arctic Aerosol Pollution during Winter−Spring, Environ. Sci. Technol., 43 (2), 286-292, 2008.

Geng, H., Ryu, J., Jung, H.-J., Chung, H., Ahn, K.-H., Ro, C.-U.: Single-Particle Characterization of Summertime Arctic Aerosols Collected at Ny-Alesund, Svalbard, Environ. Sci. Technol., 44 (7), 2348-2353, 2010.

Ghosal, S., Weber, P.K., Laskin, A.: Spatially resolved chemical imaging of individual atmospheric particles using nanoscale imaging mass spectrometry: insight into particle origin and chemistry, Analytical Methods, 6 (8), 2444-2451, 2014.

Gilgen, A., Huang, W.T.K., Ickes, L., Neubauer, D., Lohmann, U.: How important are future marine and shipping aerosol emissions in a warming Arctic summer and autumn?, Atmos. Chem. Phys., 18 (14), 10521-10555, 2018.

Hansen, J., Nazarenko, L.: Soot climate forcing via snow and ice albedos, P. Natl. Acad. Sci. USA, 101 (2), 423-428, 2004.

Hara, K., Yamagata, S., Yamanouchi, T., Sato, K., Herber, A., Iwasaka, Y., Nagatani, M., Nakata, H.: Mixing states of individual aerosol particles in spring Arctic troposphere during ASTAR 2000 campaign, J. Geophys. Res., 108 (D7), 2003.

Hegg, D.A., Warren, S.G., Grenfell, T.C., Sarah, J.D., Clarke, A.D.: Sources of light-absorbing aerosol in arctic snow and their seasonal variation, Atmos. Chem. Phys., 10 (22), 10923-10938, 2010.

Herrmann, A.M., Ritz, K., Nunan, N., Clode, P.L., Pett-Ridge, J., Kilburn, M.R., Murphy, D.V., O'Donnell, A.G., Stockdale, E.A.: Nano-scale secondary ion mass spectrometry — A new analytical tool in biogeochemistry and soil ecology: A review article, Soil Biol. Biochem., 39 (8), 1835-1850, 2007.

IPCC (2013), Clouds and Aerosols, in Climate Change 2013: The Physical Science Basis. Contribution

of Working Group I to the Fifth Assessment Report of the Intergovernmental Panel on Climate Change, 571-657 pp, Cambridge, U.K. and New York, NY.

Iwasaka, Y., Minoura, H., Nagaya, K.: The transport and spatial scale of Asian dust-storm clouds: A case study of the dust-storm event of April 1979, Tellus, Ser. B, 35, 189-196, 1983.

Iziomon, M.G., Lohmann, U., Quinn, P.K.: Summertime pollution events in the Arctic and potential implications, J. Geophys. Res., 111 (D12), D12206, 2006.

Jacob, D.J., Crawford, J.H., Maring, H., Clarke, A.D., Dibb, J.E., Emmons, L.K., Ferrare, R.A., Hostetler, C.A., Russell, P.B., Singh, H.B., Thompson, A.M., Shaw, G.E., McCauley, E., Pederson, J.R., Fisher, J.A.: The Arctic Research of the Composition of the Troposphere from Aircraft and Satellites (ARCTAS) mission: design, execution, and first results, Atmos. Chem. Phys., 10 (11), 5191-5212, 2010.

Jiang, H., Frie, A.L., Lavi, A., Chen, J.Y., Zhang, H., Bahreini, R., Lin, Y.-H.: Brown Carbon Formation from Nighttime Chemistry of Unsaturated Heterocyclic Volatile Organic Compounds, Environ. Sci. Techn. Lett., DOI: 10.1021/acs.estlett.1029b00017, 2019.

Karl, M., Leck, C., Coz, E., Heintzenberg, J.: Marine nanogels as a source of atmospheric nanoparticles in the high Arctic, Geophys. Res. Lett.,, 40 (14), 3738-3743, 2013.

Kirpes, R.M., Bondy, A.L., Bonanno, D., Moffet, R.C., Wang, B., Laskin, A., Ault, A.P., Pratt, K.A.: Secondary sulfate is internally mixed with sea spray aerosol and organic aerosol in the winter Arctic, Atmos. Chem. Phys., 18 (6), 3937-3949, 2018.

Koch, D., Hansen, J.: Distant origins of Arctic black carbon: A Goddard Institute for Space Studies ModelE experiment, J. Geophys. Res., 110 (D4), D04204, 2005.

Lack, D.A., Langridge, J.M., Bahreini, R., Cappa, C.D., Middlebrook, A.M., Schwarz, J.P.: Brown carbon and internal mixing in biomass burning particles, P. Natl. Acad. Sci. USA, 109 (37), 14802-14807, 2012.

Laskin, A., Laskin, J., Nizkorodov, S.A.: Chemistry of Atmospheric Brown Carbon, Chem. Rev., 115 (10), 4355-4382, 2015.

Laskina, O., Morris, H.S., Grandquist, J.R., Estillore, A.D., Stone, E.A., Grassian, V.H., Tivanski, A.V.: Substrate-Deposited Sea Spray Aerosol Particles: Influence of Analytical Method, Substrate, and Storage Conditions on Particle Size, Phase, and Morphology, Environ. Sci. Tech., 49 (22), 13447-13453, 2015.

Lathem, T.L., Beyersdorf, A.J., Thornhill, K.L., Winstead, E.L., Cubison, M.J., Hecobian, A., Jimenez, J.L., Weber, R.J., Anderson, B.E., Nenes, A.: Analysis of CCN activity of Arctic aerosol and Canadian biomass burning during summer 2008, Atmos. Chem. Phys., 13 (5), 2735-2756, 2013.

Law, K.S., Stohl, A.: Arctic Air Pollution: Origins and Impacts, Science, 315 (5818), 1537-1540, 2007.

Leck, C., Bigg, E.K.: Comparison of sources and nature of the tropical aerosol with the summer high Arctic aerosol, Tellus, Ser. B, 60 (1), 118-126, 2008.

Leck, C., Svensson, E.: Importance of aerosol composition and mixing state for cloud droplet activation over the Arctic pack ice in summer, Atmos. Chem. Phys., 15 (5), 2545-2568, 2015.

Li, W., Sun, J., Xu, L., Shi, Z., Riemer, N., Sun, Y., Fu, P., Zhang, J., Lin, Y., Wang, X., Shao, L., Chen, J., Zhang, X., Wang, Z., Wang, W.: A conceptual framework for mixing structures in individual aerosol particles, J. Geophys. Res., 121 (22), 13,784-713,798, 2016.

Li, W., Xu, L., Liu, X., Zhang, J., Lin, Y., Yao, X., Gao, H., Zhang, D., Chen, J., Wang, W., Harrison, R.M., Zhang, X., Shao, L., Fu, P., Nenes, A., Shi, Z.: Air pollution–aerosol interactions produce more bioavailable iron for ocean ecosystems, Sci. Adv., 3 (3), e1601749, 2017.

Maahn, M., de Boer, G., Creamean, J.M., Feingold, G., McFarquhar, G.M., Wu, W., Mei, F.: The observed influence of local anthropogenic pollution on northern Alaskan cloud properties, Atmos. Chem. Phys., 17 (23), 14709-14726, 2017.

Martin, M., Chang, R.Y.W., Sierau, B., Sjogren, S., Swietlicki, E., Abbatt, J.P.D., Leck, C., Lohmann, U.: Cloud condensation nuclei closure study on summer arctic aerosol, Atmos. Chem. Phys., 11 (22), 11335-11350, 2011.

Moffet, R.C., Rödel, T.C., Kelly, S.T., Yu, X.Y., Carroll, G.T., Fast, J., Zaveri, R.A., Laskin, A., Gilles, M.K.: Spectro-microscopic measurements of carbonaceous aerosol aging in Central California, Atmos. Chem. Phys., 13 (20), 10445-10459, 2013.

Moore, R.H., Bahreini, R., Brock, C.A., Froyd, K.D., Cozic, J., Holloway, J.S., Middlebrook, A.M., Murphy, D.M., Nenes, A.: Hygroscopicity and composition of Alaskan Arctic CCN during April 2008, Atmos. Chem. Phys., 11 (22), 11807-11825, 2011.

Moroni, B., Cappelletti, D., Crocchianti, S., Becagli, S., Caiazzo, L., Traversi, R., Udisti, R., Mazzola, M., Markowicz, K., Ritter, C., Zielinski, T.: Morphochemical characteristics and mixing state of long range transported wildfire particles at Ny-Ålesund (Svalbard Islands), Atmos. Environ., 156, 135-145, 2017.

Park, K., Kim, G., Kim, J.-s., Yoon, Y.-J., Cho, H.-j., Ström, J.: Mixing State of Size-Selected Submicrometer Particles in the Arctic in May and September 2012, Environ. Sci. Technol., 48 (2), 909-919, 2013.

Peters, G.P., Nilssen, T.B., Lindholt, L., Eide, M.S., Glomsrød, S., Eide, L.I., Fuglestvedt, J.S.: Future emissions from shipping and petroleum activities in the Arctic, Atmos. Chem. Phys., 11 (11), 5305-5320, 2011.

Qi, L., Li, Q., Li, Y., He, C.: Factors controlling black carbon distribution in the Arctic, Atmos. Chem. Phys., 17 (2), 1037-1059, 2017.

Quinn, P.K., Shaw, G., Andrews, E., Dutton, E.G., Ruoho-Airola, T., Gong, S.L.: Arctic haze: current trends and knowledge gaps, Tellus B, 59 (1), 99-114, 2007.

Raatikainen, T., Brus, D., Hyvärinen, A.P., Svensson, J., Asmi, E., Lihavainen, H.: Black carbon concentrations and mixing state in the Finnish Arctic, Atmos. Chem. Phys., 15 (17), 10057-10070, 2015.

Riemer, N., West, M., Zaveri, R.A., Easter, R.C.: Simulating the evolution of soot mixing state with a particle resolved aerosol model, J. Geophys. Res., 114, doi:10.1029/2008JD011073, 2009.

Riemer, N., Ault, A.P., West, M., Craig, R.L., Curtis, J.H.: Aerosol Mixing State: Measurements, Modeling, and Impacts, Rev. Geophys., 57, https://doi.org/10.1029/2018RG000615, 2019.

Saleh, R., Hennigan, C.J., McMeeking, G.R., Chuang, W.K., Robinson, E.S., Coe, H., Donahue, N.M., Robinson, A.L.: Absorptivity of brown carbon in fresh and photo-chemically aged biomass-burning emissions, Atmos. Chem. Phys., 13 (15), 7683-7693, 2013.

Samset, B.H., Myhre, G., Herber, A., Kondo, Y., Li, S.M., Moteki, N., Koike, M., Oshima, N., Schwarz, J.P., Balkanski, Y., Bauer, S.E., Bellouin, N., Berntsen, T.K., Bian, H., Chin, M., Diehl, T., Easter, R.C., Ghan, S.J., Iversen, T., Kirkevåg, A., Lamarque, J.F., Lin, G., Liu, X., Penner, J.E., Schulz, M., Seland, Ø., Skeie, R.B., Stier, P., Takemura, T., Tsigaridis, K., Zhang, K.: Modelled black carbon radiative forcing and atmospheric lifetime in AeroCom Phase II constrained by aircraft observations, Atmos. Chem. Phys., 14 (22), 12465-12477, 2014.

Sand, M., Berntsen, T.K., Kay, J.E., Lamarque, J.F., Seland, Ø., Kirkevåg, A.: The Arctic response to remote and local forcing of black carbon, Atmos. Chem. Phys., 13 (1), 211-224, 2013.

Seinfeld, J., Pandis, S., 2006. Atmospheric Chemistry and Physics: From air pollution to climate change (2nd ed.). 1-1203 pp., John Wiley & Son, Inc., Hoboken, New Jersey.

Shindell, D.: Local and remote contributions to Arctic warming, Geophys. Res. Lett.,, 34 (14), L14704, 2007.

Sierau, B., Chang, R.Y.W., Leck, C., Paatero, J., Lohmann, U.: Single-particle characterization of the high-Arctic summertime aerosol, Atmos. Chem. Phys., 14 (14), 7409-7430, 2014.

Tobo, Y., Adachi, K., DeMott, P.J., Hill, T.C.J., Hamilton, D.S., Mahowald, N.M., Nagatsuka, N., Ohata, S., Uetake, J., Kondo, Y., Koike, M.: Glacially sourced dust as a potentially significant source of ice nucleating particles, Nature Geoscience, 12 (4), 253-258, 2019.

Updyke, K.M., Nguyen, T.B., Nizkorodov, S.A.: Formation of brown carbon via reactions of ammonia with secondary organic aerosols from biogenic and anthropogenic precursors, Atmos. Environ., 63 (0), 22-31, 2012.

Wöhrnschimmel, H., MacLeod, M., Hungerbuhler, K.: Emissions, Fate and Transport of Persistent Organic Pollutants to the Arctic in a Changing Global Climate, Environ. Sci. Technol., 47 (5), 2323-2330, 2013.

Wang, B., Laskin, A., Roedel, T., Gilles, M.K., Moffet, R.C., Tivanski, A.V., Knopf, D.A.: Heterogeneous ice nucleation and water uptake by field-collected atmospheric particles below 273 K, J. Geophys. Res., 117, 2012.

Wang, X., Heald, C.L., Liu, J., Weber, R.J., Campuzano-Jost, P., Jimenez, J.L., Schwarz, J.P., Perring, A.E.: Exploring the observational constraints on the simulation of brown carbon, Atmos. Chem. Phys., 18 (2), 635-653, 2018.

Wang, Z., Bi, L., Yi, B., Zhang, X.: How the Inhomogeneity of Wet Sea Salt Aerosols Affects Direct Radiative Forcing, Geophysical Research Letters, 46 (3), 1805-1813, 2019.

Weinbruch, S., Wiesemann, D., Ebert, M., Schütze, K., Kallenborn, R., Ström, J.: Chemical composition and sources of aerosol particles at Zeppelin Mountain (Ny Ålesund, Svalbard): An electron microscopy study, Atmos. Environ., 49 (0), 142-150, 2012.

Winiger, P., Andersson, A., Eckhardt, S., Stohl, A., Gustafsson, Ö.: The sources of atmospheric black carbon at a European gateway to the Arctic, Nat. Commun., 7, 12776, 2016.

Winiger, P., Andersson, A., Eckhardt, S., Stohl, A., Semiletov, I.P., Dudarev, O.V., Charkin, A., Shakhova, N., Klimont, Z., Heyes, C., Gustafsson, Ö.: Siberian Arctic black carbon sources constrained by model and observation, P. Natl. Acad. Sci. USA, 114 (7), E1054-E1061, 2017.

Xu, J.W., Martin, R.V., Morrow, A., Sharma, S., Huang, L., Leaitch, W.R., Burkart, J., Schulz, H., Zanatta, M., Willis, M.D., Henze, D.K., Lee, C.J., Herber, A.B., Abbatt, J.P.D.: Source attribution of Arctic black carbon constrained by aircraft and surface measurements, Atmos. Chem. Phys., 17 (19), 11971-11989, 2017.

Yang, Y., Wang, H., Smith, S.J., Easter, R.C., Rasch, P.J.: Sulfate Aerosol in the Arctic: Source Attribution and Radiative Forcing, J. Geophys. Res., 123 (3), 1899-1918, 2018.

You, Y., Renbaum-Wolff, L., Carreras-Sospedra, M., Hanna, S.J., Hiranuma, N., Kamal, S., Smith, M.L., Zhang, X., Weber, R.J., Shilling, J.E., Dabdub, D., Martin, S.T., Bertram, A.K.: Images reveal that atmospheric particles can undergo liquid–liquid phase separations, P. Natl. Acad. Sci. USA, 109 (33), 13188-13193, 2012.

Zanatta, M., Laj, P., Gysel, M., Baltensperger, U., Vratolis, S., Eleftheriadis, K., Kondo, Y., Dubuisson, P., Winiarek, V., Kazadzis, S., Tunved, P., Jacobi, H.W.: Effects of mixing state on optical and radiative properties of black carbon in the European Arctic, Atmos. Chem. Phys., 18 (19),

14037-14057, 2018.

Zangrando, R., Barbaro, E., Zennaro, P., Rossi, S., Kehrwald, N.M., Gabrieli, J., Barbante, C., Gambaro, A.: Molecular Markers of Biomass Burning in Arctic Aerosols, Environ. Sci. Technol., 47 (15), 8565-8574, 2013.

Figure Captions

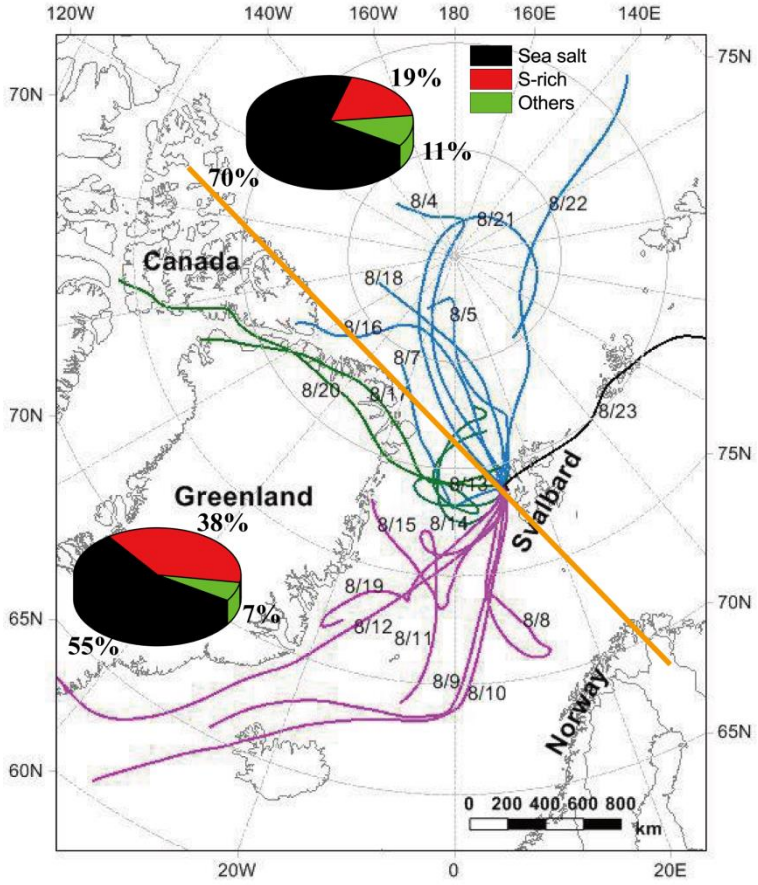

Figure 1 72 h back trajectories of air masses at 500 m over Arctic Yellow River Station in Svalbard during 3–26 August 2012, and arriving time was set according to the sampling time. Air masses were divided into two groups by the yellow line: one group from the central Arctic Ocean and the other one from North America and Greenland. Pie charts show the number fractions of sea salt, S-rich, and other particles.

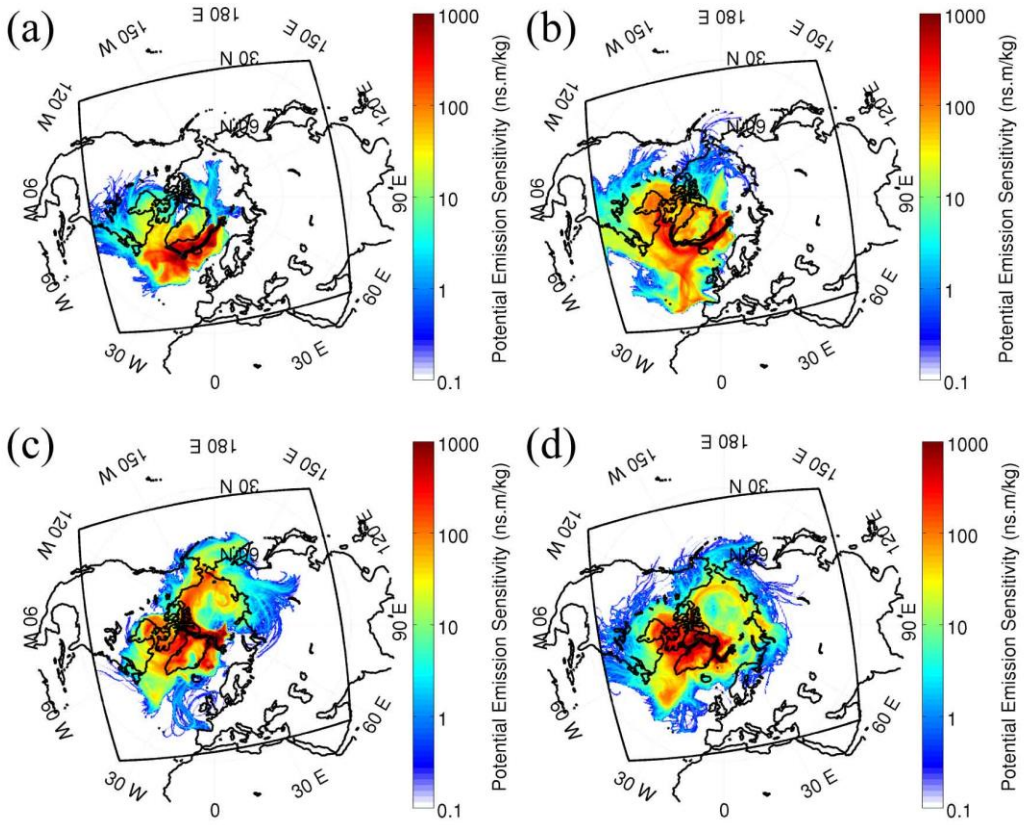

Figure 2 FLEXPART-WRF on August 11, 12, 14, and 15, 2012. Black square shows the WRF domain used to initiate the FLEXPART-WRF simulation.

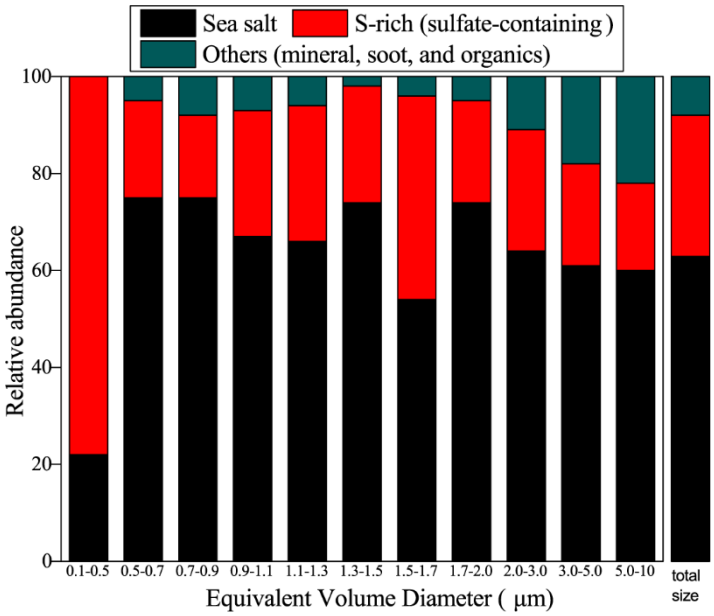

Figure 3 Relative abundances of typical individual aerosol particles in the analysed samples. Sulfate-containing particles include all particles that are internal mixture of sulfate and OM, with or without soot.

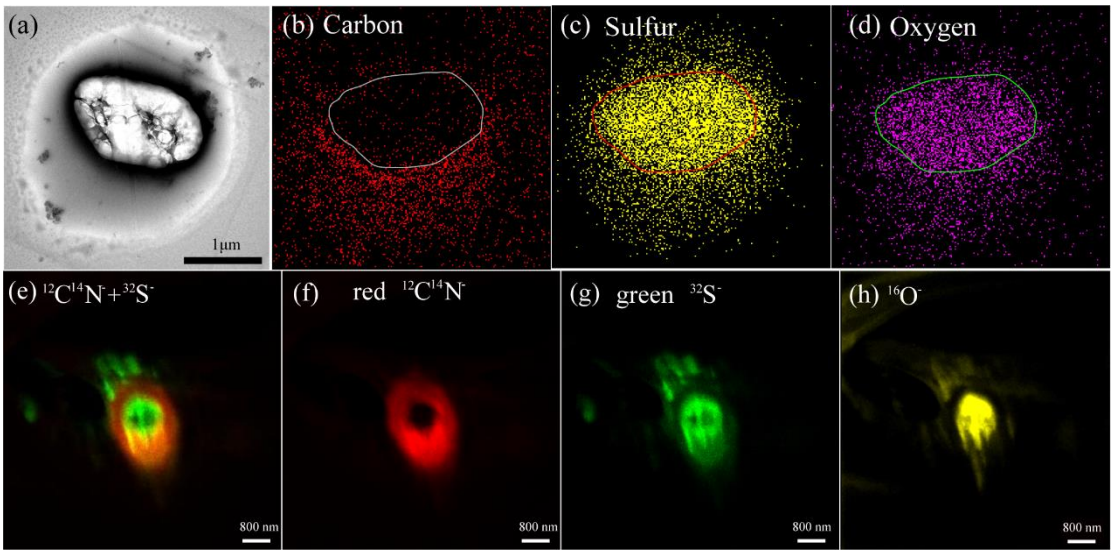

Figure 4 TEM images of a secondary particle and NanoSIMS intensity threshold maps of an aerosol particle with sulfate core and OM coating. (a) Bright-field TEM image of an internally mixed particle; (b) elemental carbon (c) sulfur and (d) oxygen maps of the internally mixed particle shown in 1(a); (e) Overlay of $^{12}C^{14}N^{-}$ and $^{32}S^{-}$ ion maps in an internally mixed particle; (f) CN^{-} map (g) S^{-} (h) O^{-} secondary ion maps. Ion maps with a set of aerosol particles were shown in Figure S1.

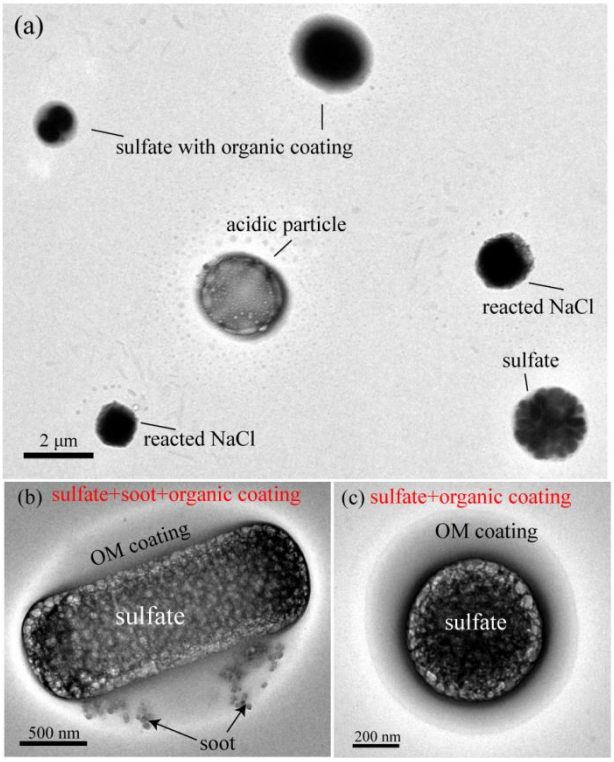

Figure 5 TEM images of individual particles containing sulfate, OM, and soot. (a) Low magnification TEM image showing sulfates, sulfate with OM coating, and reacted NaCl particles. (b) an internally mixed particle of sulfate and soot with OM coating (c) a particle with sulfate core and OM coating.

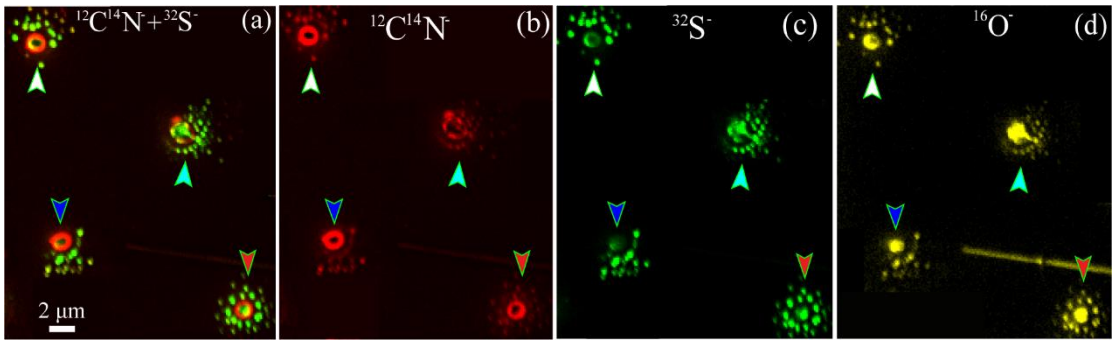

Figure 6 NanoSIMS intensity threshold maps of individual aerosol particles surrounded by satellite particles. (e) Overlay of $^{12}C^{14}N^{-}$and $^{32}S^{-}$ ion maps of individual particles. (f) CN^{-} (g) S^{-} (h) O^{-} maps. Four particles were indicated by white, pink, blue, and red arrows.

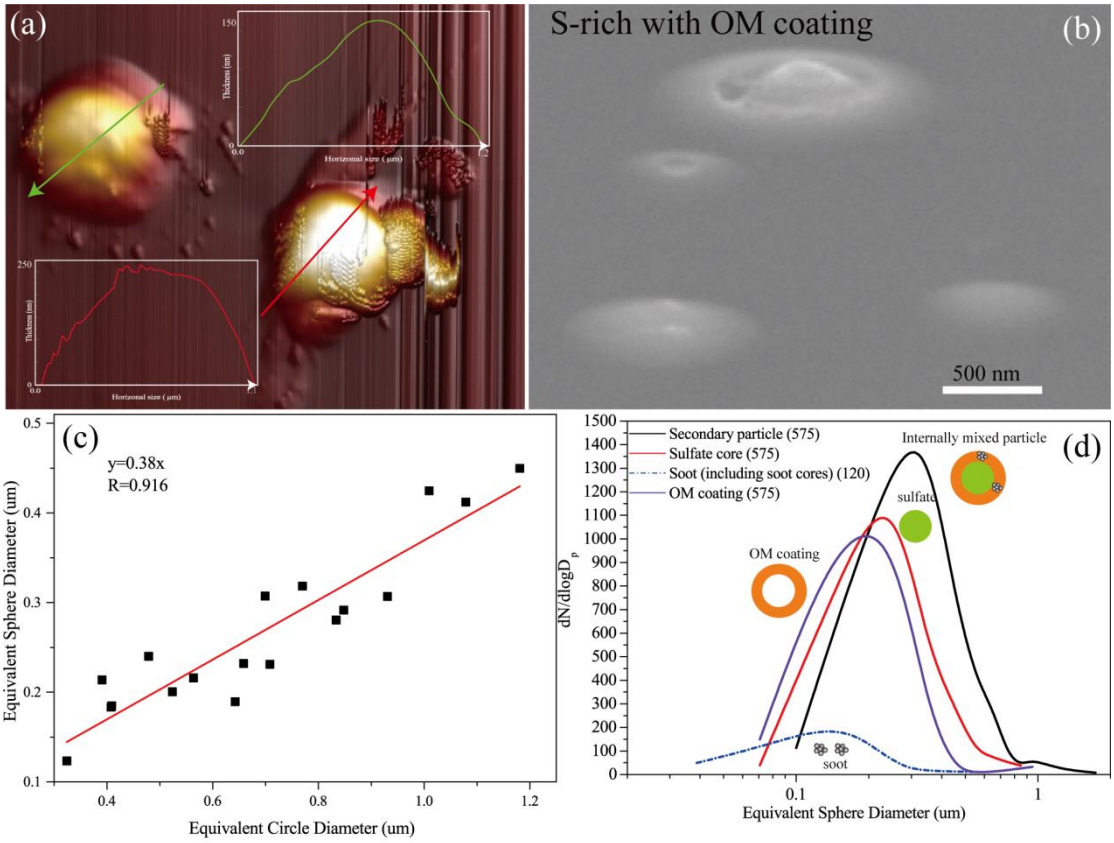

Figure 7 AFM image and calculated diameter of individual particles. (a) 3-D AFM image of sulfate-containing particles. The colored arrows represent the cross sections where the particles heights are measured (see insert figures) . (b) SEM image of S-rich particles with OM coating obtained from 75° tilt of the SEM specimen stage (c) The near linear relationships between ECD and ESD based on S-rich particles with OM coating by atomic force microscopy. (d) Size distribution of individual particle with OM coating and sulfate core based on the estimated ESD diameter from TEM image.

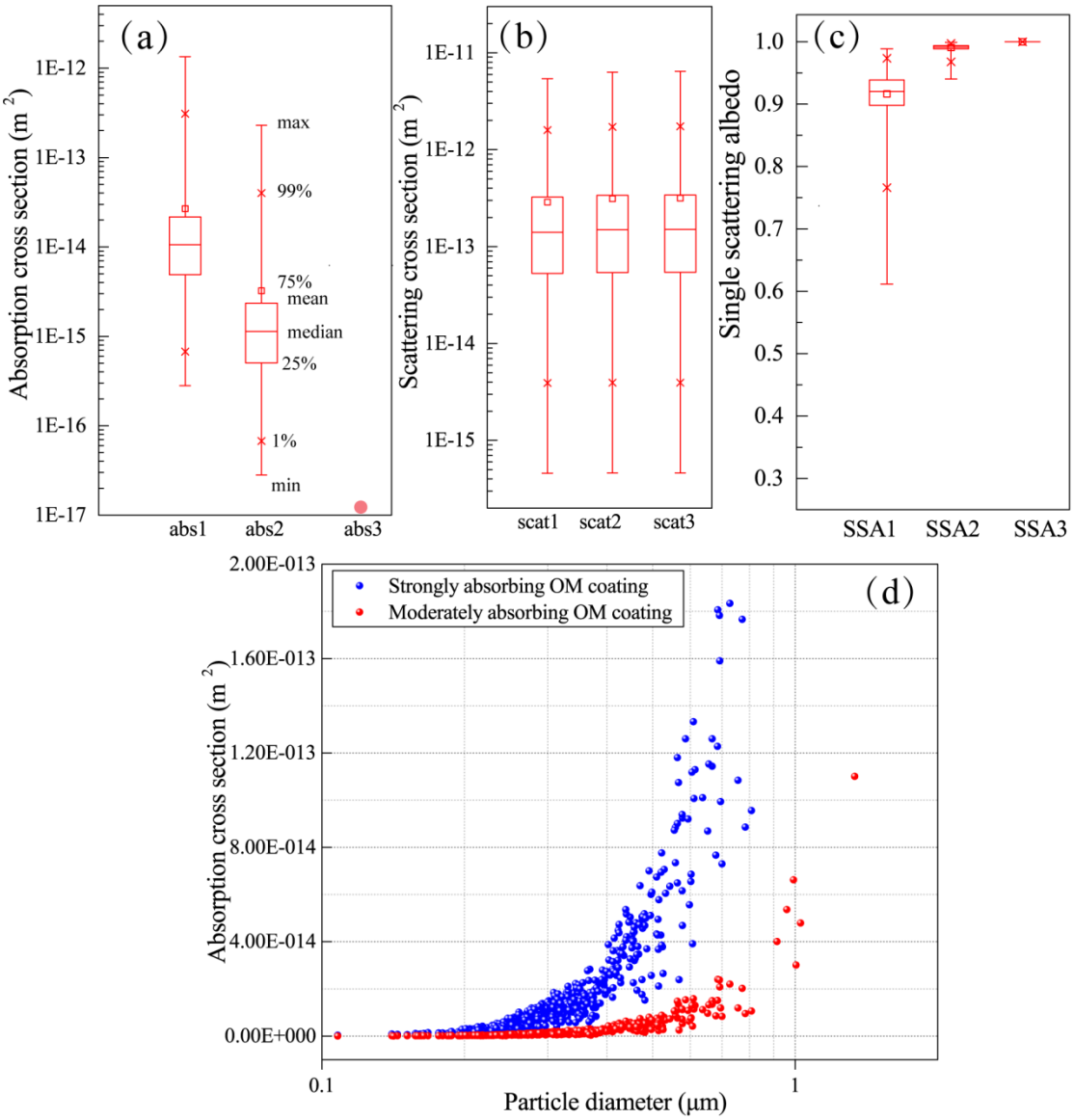

Figure 8 Optical properties of box-and-whisker plots showing optical parameters of all analysed particles assuming sulfate core and BrC shell (not considering soot cores in the particles). (a) Scattering cross section (b) Absorption cross section (c) Single scattering albedo. Top to bottom makers in the box-and-whisker represent max, 99%, 75%, mean, median, 25%, 1%, min values. (d) Absorption cross section along with particle diameter assuming strongly absorbing BrC and Moderate absorbing BrC as the particle OM coating. Abs 1, abs 2 and abs3 represent the BrC with highly, moderately and weak absorbing property.

Table 1 Sampling information in Arctic area and their analysis

Date	Local time	T	RH	P	WD	WS	TEM	EDS	SEM	AFM	NanoSIMS
2012.8.7	20:50 -21:15	4.9	84	1009.0	296	4.1	43	10			
2012.8.8	08:23 -08:48	4.9	81	1007.6	238	2.1	38	11			
2012.8.9	14:40 -15:05	6.6	81	1003.9	129	6.5	146	50			12
	15:20 -15:49	7.0	78	1003.5	120	7.3	130	26	20		
2012.8.10	00:15 -00:40	7.3	80	998.6	135	8.9	121	23			
2012.8.11	09:10 -09:35	6.2	94	997.0	303	3.3	128	50			10
2012.8.11	16:00 -16:25	4.1	92	1002.0	327	4.6	156	55		6	
2012.8.12	15:25 -15:50	5.7	83	1006.8	132	6.9	100	15	32		
2012.8.13	08:55 -09:20	5.3	81	1009.6	91	1.1	113	16			
2012.8.13	14:15 -14:40	4.5	90	1011.4	351	2.1	136	56			10
2012.8.14	09:50 -10:20	5.0	85	1019.7	351	2.3	134	24			
2012.8.14	15:12 -15:42	4.6	88	1020.5	117	2.6	121	26			
2012.8.14	21:17 -21:47	4.8	84	1020.7	276	5.4	178	56		5	
2012.8.15	09:15 -09:45	5.8	73	1019.6	135	3.7	165	60		6	
2012.8.15	15:00 -15:33	6.8	70	1018.9	270	3.3	80	11			
2012.8.17	9:00 -10:00	3.8	86	1017.1	116	0.3	30	15			
2012.8.17	14:50 -15:20	3.7	85	1015.7	109	2.2	42	16			
2012.8.21	15:05 -15:40	1.6	87	1003.7	314	6.8	46	18			
2012.8.22	08:55 -09:30	2.8	78	999.2	331	2.8	49	19			
2012.8.23	09:00 -09:40	3.4	64	998.0	136	6.9	21	9			
2012.8.23	20:35 -21:08	3.8	59	1002.0	138	6.3	25	9			